7.5.2 Analysis of reflections

In the simple model of the string (Chapter 1), two transversal waves propagate along the string after it is being plucked (**Fig. 7.15**, left). Let us take as stimulus a short impulse (at A) that – in the ideal case – is reflected at both bearings with opposite phase. The corresponding idealized time function at the observation point (B) is seen on the right. In reality, we get large deviations from this idealized model: the propagation of transversal waves is dispersive (Chapter 1.3), and at the bearings there is both a loss of vibration energy and an exchange of energy between transversal waves and longitudinal waves. This exchange is the subject of the following elaborations based on measurements that targeted the development of a more precise reflection model.

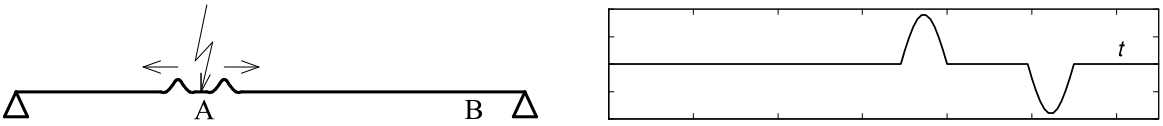

Fig. 7.15: Simple model for transversal waves: impulse excitation at A (left); time function at B (right).

If the time function appearing at B (in Fig. 7.15) were as simple as depicted in the graph, it would be easy to distinguish between the wave running forwards and the wave running backwards, and to determine a reflection factor. However, due to the frequency dependency of the group delay (**dispersion**), short impulses get broadened already after a few centimeters into a **chirp** such that we get a mix of the two waves running to and from (**Fig. 7.16**).

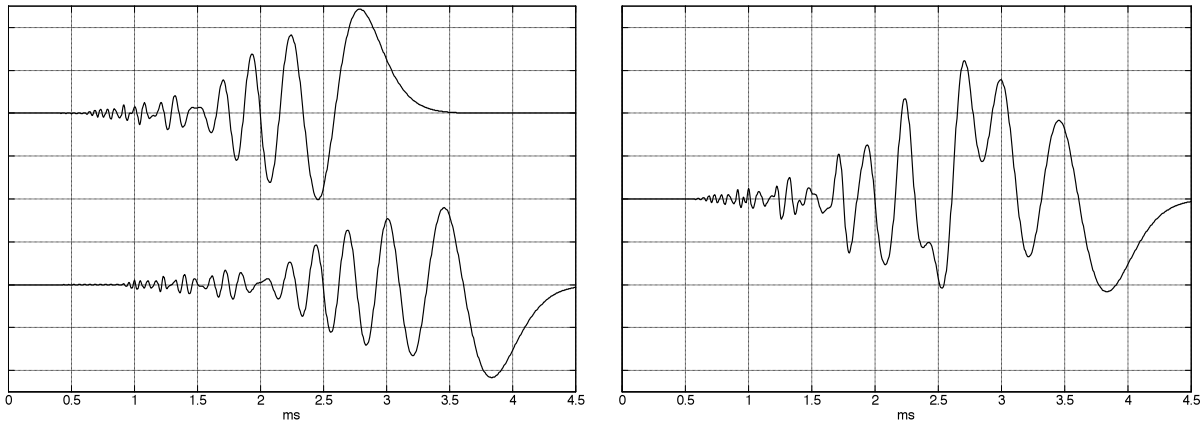

Fig. 7.16: Forwards- and backwards-running waves at point B, with dispersion (left); superposition at B (right).

If the requirements with regard to accuracy are not too high, it is possible to de-convolve one of the two waves, and in the end to obtain a separation with respect to time, after all. To do this, the string is interpreted as a linear, time-invariant system (Chapters 1 and 2), the output signal of which is a convolution of input signal and impulse response. For small displacements, assuming linearity provides a very reasonable approximation. Time-invariance can be obtained only for short durations of time due to unavoidable temperature changes. From output signal and impulse response, the **de-convolution** (as the inverse operation of convolution) yields the input signal. The latter could be a short impulse (at A), while the output signal is the measurement result determined at B (e.g. the particle velocity), and the impulse response can be calculated on the basis to the string data (Chapter 1). However, as elegant as this approach may be in theory, in practice we quickly recognize new problems: the signal energy delivered via a short impulse is small, and therefore a lot of noise but only little useful signal arrive at the measuring point. The de-convolution is correspondingly impaired.

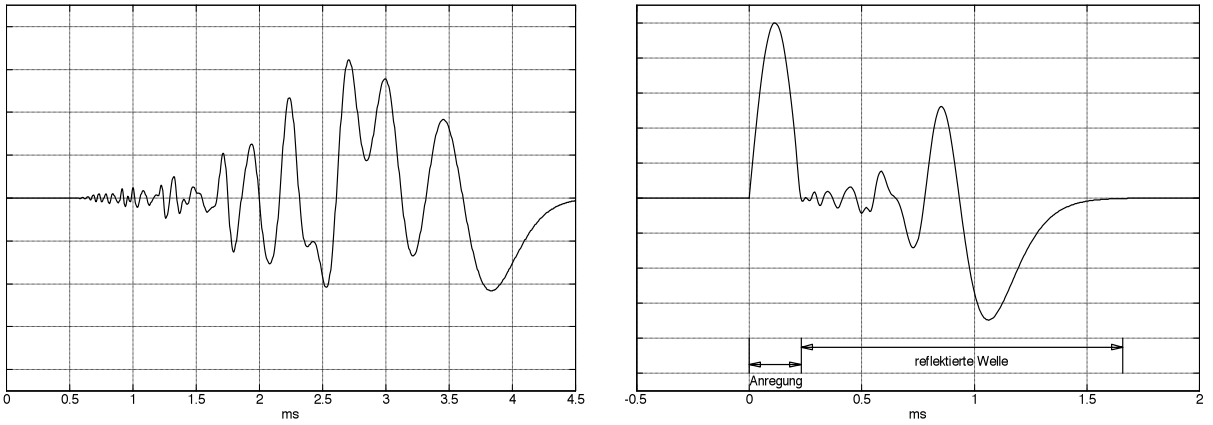

Fig. 7.17: Summation signal at B (left), de-convolution (right). Both curves are calculated, not measured. "Anregung" = excitation; "reflektierte Welle" = reflected wave.

Fig. 7.17 indicates how all this would work in **theory**: via de-convolution of the output signal at B (left section of the figure) with the inverse impulse response that maps from A to B, the (positive) output impulse is retrieved. The reflection is added in – it is not fully de-convoluted because it has run a longer distance, after all. After separating the signal, though, the reflection could also be de-convoluted back right up to the excitation impulse.

However, as has already been mentioned, excitation with a short impulse has its problems: the useable signal dynamic is small. We get better results if we excite the string at point A using a special chirp, the mapping of which onto B results in a short impulse. The excitation signal A thus needs to be configured exactly such that its dispersive mapping onto B yields a short impulse that can easily be separated from the subsequent reflections (**Fig. 7.18**).

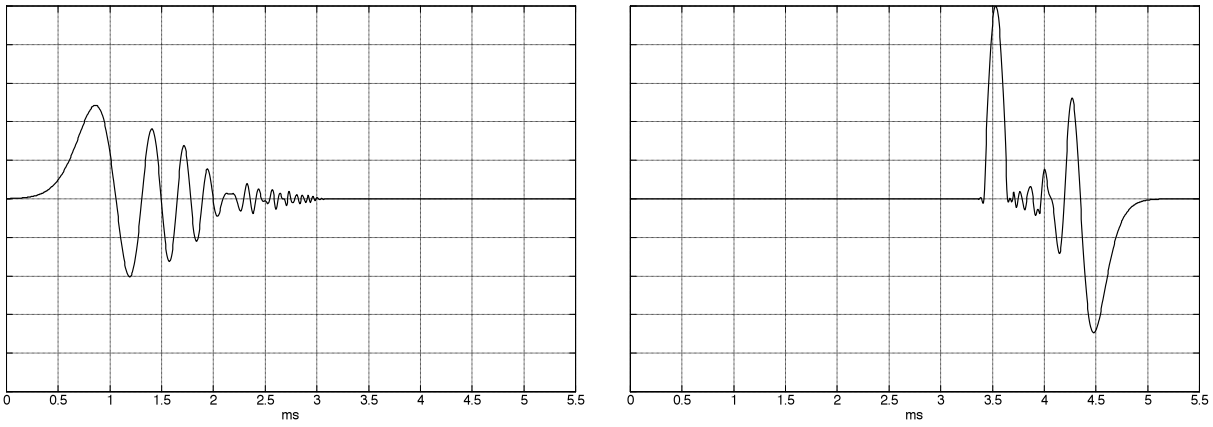

Fig. 7.18: Excitation chirp at A (left), output signal at B (right); model calculation.

In contrast to the model calculations elaborated so far, we now turn to **measurements** with an experimental setup. A string a length of 13 m length *(translators note: no kidding!)* made of steel wire at 0.7 mm diameter was tensioned to yield a fundamental frequency of 6 Hz. It was deflected transversally with a chirp using a shaker (B&K 4810). Since the transmission characteristic of the shaker is frequency-dependent, the chirp depicted in Fig 7.18 needed to be pre-filtered once more, such that the forward-running wave shaped up to a half-sine impulse at a distance of 3 m. This can only be achieved as an approximation because a time-limited impulse would require a infinitely broad spectrum; bandwidth-limiting to technically feasible ranges leads to a broadening of impulses – to spurious oscillations, specifically. After some lengthy optimization work, a usable compromise could be found that delivered reliable measurement results, after all.

The experimental setup is shown in **Fig. 7.19**: the 13.3-m-long string runs across a knife-edge bearing and to its end-fixture 10 cm away. The bend angle at the knife-edge is adjustable. Via a chirp generated by a B&K 4810 shaker, the string receives excitation to oscillate transversally. At about 20 cm distance from the knife-edge, the transversal velocity of the string is measured using a laser vibrometer. The chirp is calculated such that the transversal wave running towards the right generates a velocity impulse of half-sine shape.

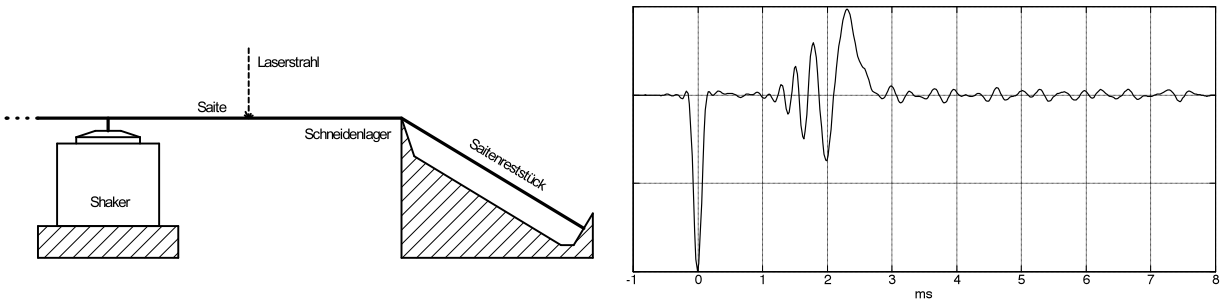

Fig. 7.19: Reflection-measurement setup. Length of the residual string ("Saitenreststück"): 10 cm; distance between knife-edge bearing ("Schneidenlager") and access point for laser beam ("Laserstrahl"): about 20 cm; distance between measuring point and shaker: about 3 m. The string ("Saite"; ∅ 0.7 mm, overall length 13.3 m) is tuned to a fundamental of about 6 Hz. Right: time function of the velocity measured via the laser vibrometer.

The scaling in Fig. 7.19 (right-hand section) is such that the (negative) excitation impulse happens around 0 s on the time axis, accompanied by some minor spurious oscillations. From about 1 ms, the dispersively broadened reflection becomes visible, and from about 3 ms, vibrations caused by the residual part of the string become apparent. Only for a string without any bending-stiffness would the two sections of the string remain completely decoupled via the motion-free bearing. Given a string with bending-stiffness, a coupling of the vibration does happen with such a bearing, as well (Chapter 2.7). The bearing is able to take on transversal forces but cannot absorb the bending moments that also occur in a flexural wave – these moments are transmitted across the bearing to the respective other section of the string. The length of the residual string (98 mm) corresponds to a fundamental frequency of 920 Hz; at this frequency and its "multiples", energy is withdrawn from the reflection. The term "multiple" should not be taken entirely literally here because the Eigen-frequencies are spread out dispersively. In **Fig. 7.20**, the de-convolved impulses running back and forth are shown, and also the spectra for the two functions. Apart from the many ripples representing analysis artifacts, two peculiarities can clearly be recognized in the **spectrum of the reflection**: the unexpectedly high damping (attenuation) of the reflection (on average about 1 dB), and selective minima at the Eigen-frequencies of the residual part of the string.

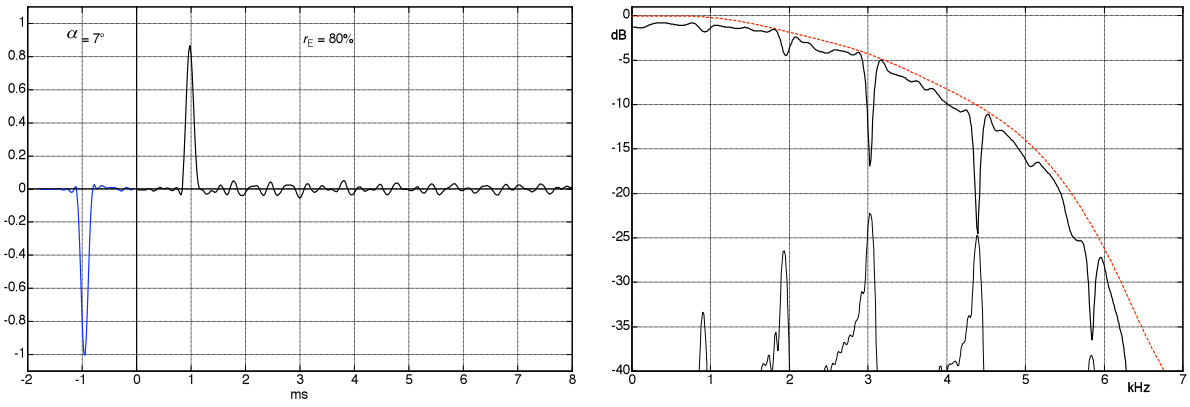

Fig. 7.20: De-convolved reflectogram (left): excitation spectrum (----), reflection spectrum (——). On the right, the velocity-spectrum of the vibration of the residual string is represented as the thin line.

Previous experiments had already shown that a bending-coupling was happening across the knife-edge bearing, and that vibration energy was withdrawn from the string selectively (Chapter 2). It is, however, surprising that the energy of the wave reflected by the bearing is 20% less than the energy of the wave running towards the bearing. If indeed the wave would loose 20% of its energy at each reflection, a 500-Hz-vibration would be attenuated by 48 dB already after 0.1 s – this contradicts any real experience. Justifiably, the spectral distribution of the reflected energy may be questioned because every short-term spectrum will include artifacts. The time-function of the velocity measured via the laser (Fig. 7.19) is much more reliable, though. If the **degree of energy-reflection** remains so clearly below the expected value (assumed at possibly 98%), then there are two possibilities for errors: either the measurement of the excitation energy yields is too high a value, or that of the reflection yields one too low. An error regarding the excitation energy can by and large be excluded: the summation of the squared signal happens across merely one 1 ms – at that point no reflection has happened. For the reflected energy, however, the situation is different: theoretically it would be possible that the excitation is not concentrated in the impulse shown in the figure, but includes an additional component that is in opposite phase to the subsequent reflection. This highly unlikely scenario could be excluded, as well, by modifying the parameters: all measurements gave a degree of energy-reflection of 80%, calculated from the time function.

Changing the **bend angle of the strings** (across the knife edge) shows us where the seemingly lost energy goes. For the first measurements this angle (that indicates the change of direction of the string at the knife edge) amounted to α = 7°. In a second series of experiments, α was increased to 23°, resulting in a further reduction of the degree of reflection to only 68%. However, for these measurements, 5 ms after the first reflection a further, smaller reflection appears, and this provides the key to understanding. The overall length of the string used for the measurements was 13.3 m: with v_D = 5200 m/s, an **expansion wave** (longitudinal wave, dilatational wave) needs 5.1 ms to run back and forth two times (without dispersion!). Evidently, the transversal wave arriving at the knife-edge bearing is transformed (to a non-negligible degree) into a longitudinal wave that runs quickly and dispersion-free to the other end of the string. There, it is reflected partially as longitudinal wave, and partially as transversal wave. Crucial in the present context is the reflected longitudinal wave: it returns after 5.1 ms and releases a secondary transversal wave at the knife-edge bearing. With the laser only detecting transversal waves, the longitudinal wave remains invisible. That a longitudinal wave is in fact generated is easily verified using a force sensor measuring the longitudinal force at the end of the string: indeed, exactly between the two reflections depicted in Fig. 7.22, we get an impulse of longitudinal force (not included in the drawing, see Fig. 7.29).

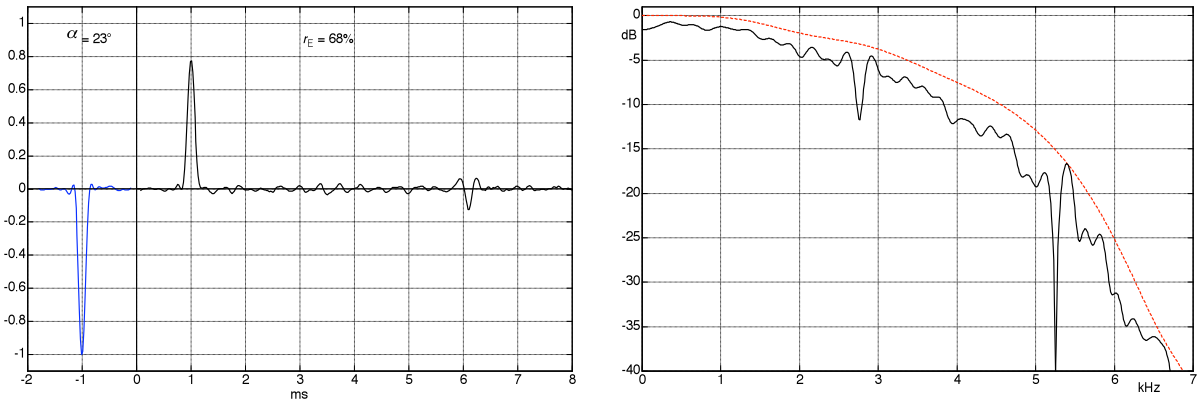

Fig. 7.21: As Fig. 7.20 but with the bend-angle of the string increased to α = 23°.

The results so far can be summarized as the following insight: the stronger the string changes direction at the bearing (i.e. the larger the bend angle is), the more efficiently the transformation from transversal to longitudinal vibration energy will be at the bearing. More concisely: **the more pronounced the bend, the stronger the mode-coupling**. Two more experiments are to deliver support for this hypothesis: in **Fig. 7. 22**, the bend angle was enlarged to 45° – a value typically found in a Stratocaster. The degree of reflection decreased to 59%, the 5-ms-reflection becomes even stronger.

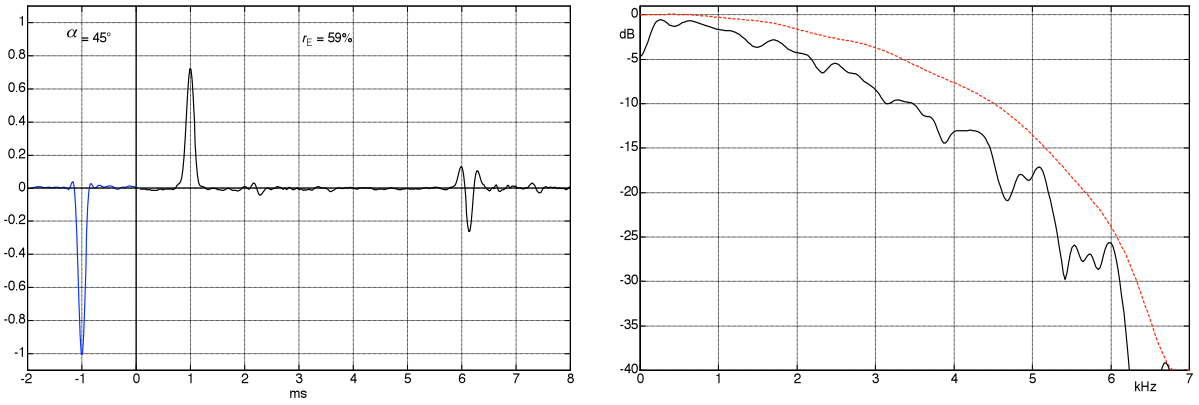

Fig. 7.22: As Fig. 7.20 but with the bend-angle of the string increased to $\alpha = 45°$.

As the other extreme, the measurement doing away with any bend angle concludes the experiments – the string simply ends in a heavy brass block without previously crossing a bridge (**Fig. 7.22)**. The degree of reflection calculated from the measurement is 99%, with a 5-ms-relection not identifiable. All these analyses allow but one conclusion: for the vast majority of electric guitars, the wave reflection at the bridge does not bother about any textbook teaching! The function of the guitar bridge, ideally assumed to be a stiff bearing or, more realistically, modeled as transverse impedance (or admittance), is more complex than assumed so far. On top of its dispersive characteristics that have not been examined yet in the present context, it acts as interface between transversal and longitudinal waves – with a degree of energy coupling up to 40% … not a negligible order of magnitude anymore. What follows for the **sound of the guitar** is this: the string vibrates not only with the Eigen-frequencies (natural frequencies) for the transversal wave but also with those for the longitudinal wave, and in addition mixed modes are possible, as well (e.g. a wave running in one direction as transversal wave and backwards as longitudinal wave). In the spectrum, we therefore expect deviations relative to the Eigen-frequencies of the rigid string.

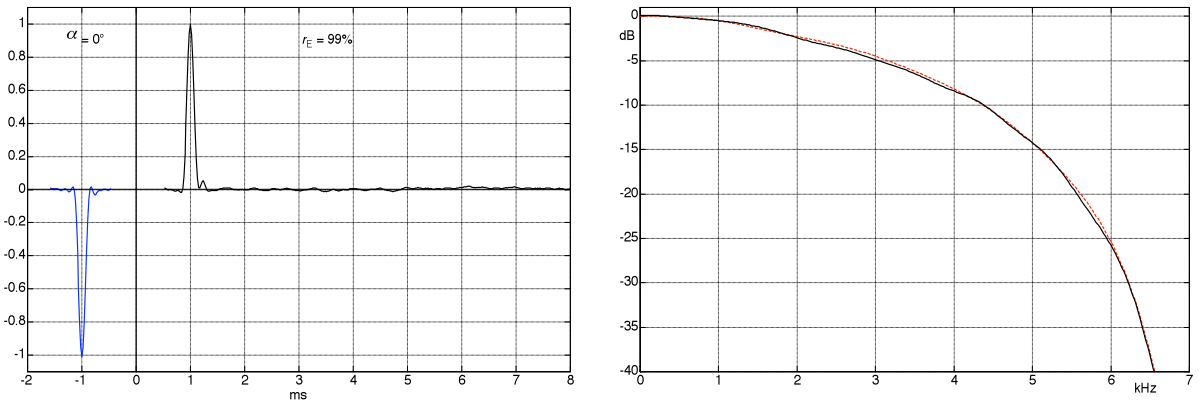

Fig. 7.23: As Fig. 7.20 but without any bend angle of the string.

Fig. 7.24 once more compiles all four of the measured reflectograms. Established scientific consensus is that reflection needs to happen with opposite phase – this is fully confirmed. However, the dependency of the amplitude of the reflected impulse on the bend angle of the string requires an extension of the usual models by a bearing-specific mode-coupling.

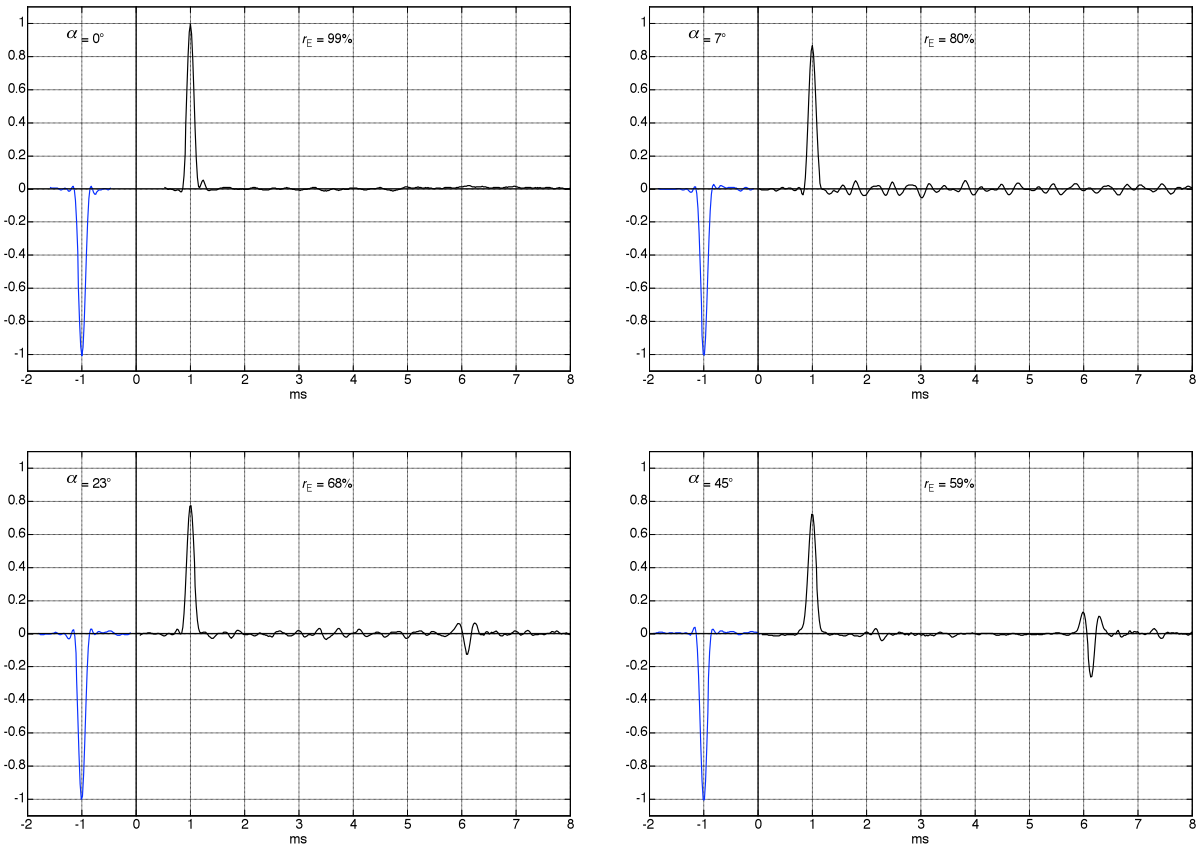

Fig. 7.24: Compilation of all reflectograms. α = bend-angle of the string; Saite, r_E = degree or energy-reflection.

Checking out popular guitar model shows that the manufacturers take advantage of the possibilities of varying the bend angle of the string: the range goes from about 4° to 45°. For the purely acoustic archtop guitars with their convex tops, choosing the bend angle was kind-of walking the tightrope between string buzz and a collapsing top: the more pronounced the bend angle, the bigger the forces acting onto the top. Given an (overall) string pull of 1000 N it is clear that the bend angle must not be too big. Some electric guitars adopted the basic build of the arched, unsupported top (Byrdland, ES-330, Tennessean, Casino), and imported the shallow bend angle, as well. With the introduction of the reinforced top (e.g. the "sustain block" in the ES-335), stability problems should in fact have been part of the past – but during the 1960s and 1970s, the ES-335 sported the trapeze tailpiece (a string fixture extending to the endpin, similar to that of the ES-330). Probably, this was for cosmetic reasons. For solid-body guitars such as the Jazzmaster and the Jaguar, the reason for the shallow bend angle was the vibrato system that was supposed to be free of detuning (with the help of the point-support bearing of the bridge). At Fender, they could have calculated that this construction would not be the best solution – but they left the market to decide. Which the marked did – without much mercy, even though these guitars were Fender's top-of-the-line models. In its first edition, the Telecaster had a steep bend angle (string-through-body), but in 1959 this was changed towards a smaller angle (top-loading). In 1960, both versions were available and after that, the steep angle was back again exclusively. One of the most pronounced bend angles is found on the Stratocaster and its countless copies.

Fig. 7.25 shows some examples of typical bridge designs. The Stratocaster bridge is available with bridge saddles of bent sheet-metal, or with solid bridge saddles, and also with vibrato or without it ("hard tail"), and in other variations not shown here. Gibson's mainstay, the Tune-O-Matic bridge is found in two versions: with the heads of the adjustment screws pointing towards the headstock, or towards the tailpiece. For the latter configuration (pictured on the left), the residual strings can make contact to the screw-heads! The bridge variant shown for the 1952 Les Paul is the one found in Lester Polfuss's patent application; the production model, however, wrapped the string under the bridge. The bridge of a 1952 Les Paul is solidly anchored into the guitar body; it could be almost seen as a solidly fixed bearing. However, since the strings could not individually be adjusted in length, Gibson introduced their Tune-O-Matic bridge in 1954 for almost all their guitars.

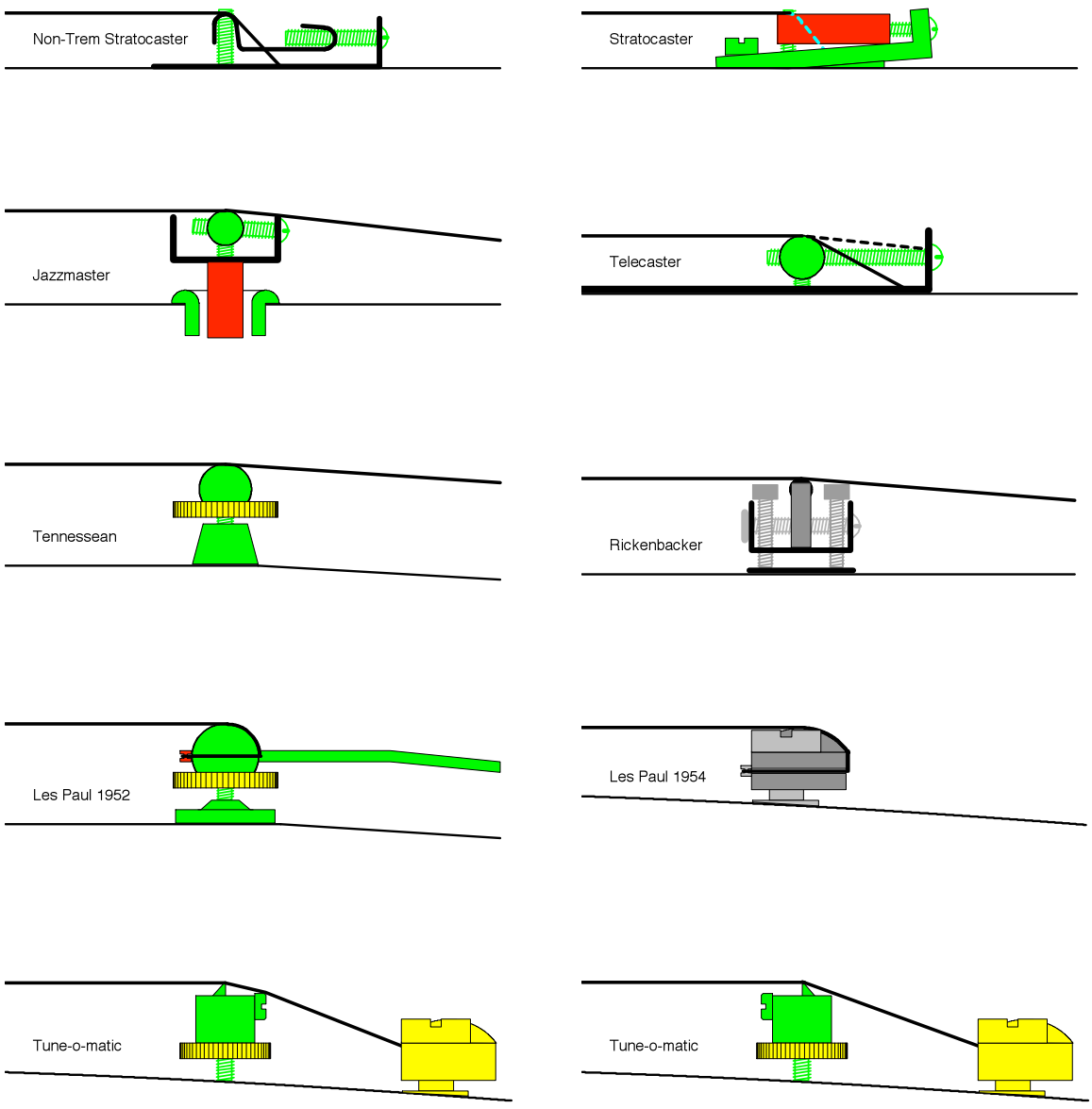

Fig. 7.25: Cross-sections of some selected guitar bridges.

We can see from Fig. 7.25 that the **bend angle of the strings** turns out rather differently between the various guitar types. Moreover, the length of the **residual section of the string**, i.e. the section between bridge and tailpiece, needs to be considered – it does make for selective absorptions. The latter are not particularly conspicuous in themselves but need to be mentioned for the sake of completeness. From the relationship between the length of the remaining string and the scale, it would be easy to estimate the resonance frequencies of the residual strings: at these frequencies, energy is withdrawn from the main section of the string – due to the bending-stiffness coupling across the bridge. The mentioned relationship is specific to the guitar type (**Fig. 7.26**), and sometimes even specific to the year of manufacture. If the length-relation is e.g. 10%, the fundamental of the resonance provided by the residual part of the E_2-string will be 824 Hz. In practice, there will be small deviations, because, for one, the bending stiffness makes for a stronger detuning for shorter strings, and also because the mounting of the strings in the tailpiece is not ideally rigid. **Fig. 7.26** depicts, as a typical example, the trapeze tailpiece of the Gibson ES-335; the table on the right gives an impression of the common length relationships.

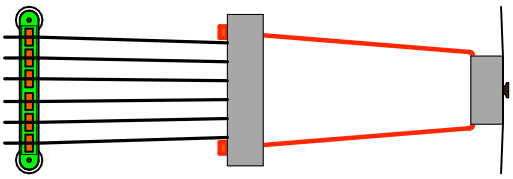

Length or residual part of string vs. scale length	
Gibson ES 140	6 %
Gibson ES 330	10 %
Gibson ES 335	17 %
Fender Jazzmaster	19 %
Gibson Byrdland	20 %

Fig. 7.26: Typical bridge with a long residual part of the string (Gibson ES 335 w/trapeze-tailpiece).

Already the few examples shown above indicate how different the build of guitar bridges may be, with corresponding differences in their influence on the string vibration. The measurements document unequivocally *that* a significant coupling of modes happens at the bridge. In the following we shall investigate in depth *why* this happens. In particular, the bend in the string requires a more exact documentation. The bend angle merely specifies the tangential (asymptotical) directions but not how the bend evolves locally across the bridge saddle. There are two extreme cases: either the string is smoothly bent across the bridge in a round just as much as is required to achieve the bend angle, or a sharp bend is introduced to the string at the bridge. The former leads to a **reversible deformation** in the case of not too big a bend, the latter brings an irreversible kink (plastic deformation) that remains even after removing any tension. **Fig. 7.27** represents both these cases for a 45° bend angle.

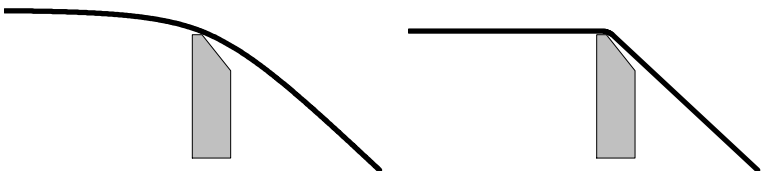

Fig. 7.27: Rounded-off and sharply-bent shape of the string for identical bend angles ($\alpha = 45°$).

For the two resulting shapes of the string, the reflection behavior is different: the rounded off shape generates a stronger coupling of modes. Apparently it is not so much the change in direction of the string but the curvature that is of significance. In the right-hand section of the figure, a strong curvature is present only directly at the bridge – but here the vibration amplitude is practically zero. In the left section of the figure, however, the curvature extends across a longer section of the string, albeit in a weaker fashion.

Reflectograms corresponding to the string geometry in Fig. 7.27 are shown in **Fig. 7.28**. The primary reflection (at 1 ms) is, compared to the more softly bent string, more pronounced for the sharply bent string. Assuming that only little energy is dissipated within the bearing for any single reflection, a weaker longitudinal wave is thus generated for the sharply bent string. The secondary reflection occurring after 6 ms qualitatively confirms this, although it has gone through an additional longitudinal/transversal coupling after the transversal/longitudinal coupling, and therefore is not a direct measure for the dilatational wave.

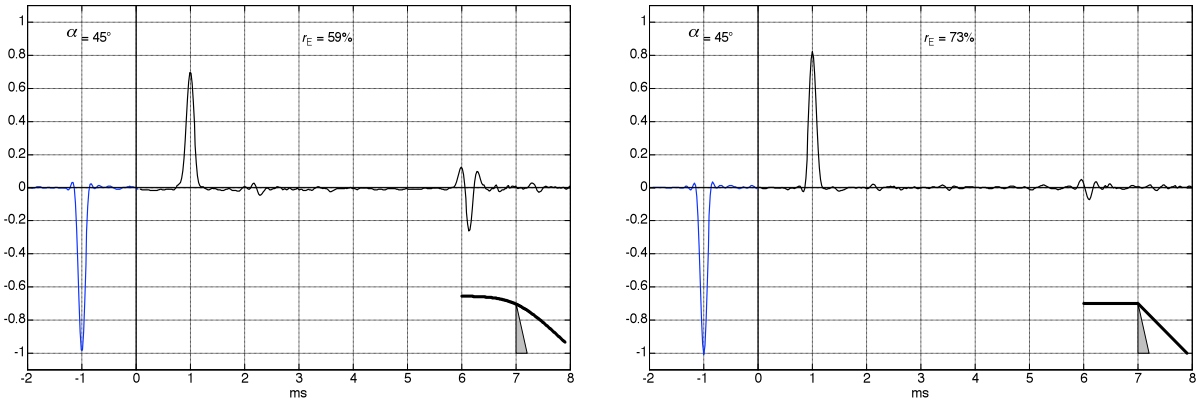

Fig. 7.28: Reflectogram for two different string curvatures; bend angle $\alpha = 45°$.

The simplest way to measure the dilatational wave generated at the bearing via the mode-coupling is using a **force sensor** that gauges the longitudinal force at the other end of the string. What needs to be considered, though, is that at a fixed bearing the motional magnitudes become zero while the forces are doubled (Chapter 2.2). Therefore, **Fig. 7.29** indicates all bearing forces only with 50% of the measured value (hoping, of course, that the bearing indeed is ideal). In order to exclude the influence of any residual part of the string, this was eliminated by anchoring the string rigidly in a rotatable cylinder. Twisting the cylinder enabled the creation of a bending moment resulting in the curvature of the string. The measurement point of the laser was located at a distance of 38 cm from the cylinder, and at another 3 m distance the shaker was positioned. Force measurements were carried out at the other end of the string where the bearing caused no curvature.

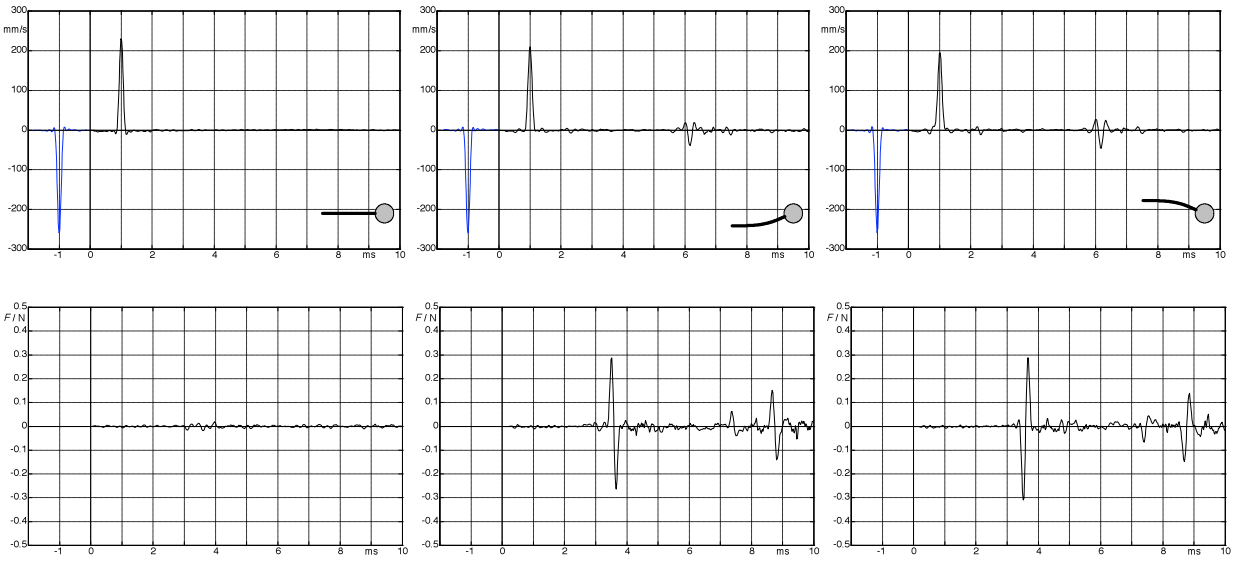

Fig. 7.29: Transversal velocity (top) and longitudinal force (bottom) for three different string curvatures.
Note: the polarity of the force signal depends on the direction of the curvature.

The measurements shown in Fig. 7.29 are impressive evidence that the mode-coupling is not the result of the presence of the residual string, but the effect of the string curvature alone. Without curvature, there is next to no longitudinal wave. If a curvature close to the bearing exists, a unipolar half-wave impulse generates a bipolar impulse that is reminiscent of a temporal differentiation. "Force = mass x differentiated velocity" would appear to be an obvious train of thought – however, the explanation proposed here points into a different direction: it's not the infinitesimal differentiation that brings us to our goal but the difference – more specifically: the superposition of the time-shifted, opposite phase signals. The velocity-wave reflected away from the bearing is in opposite phase to the wave running towards the bearing such that directly at the bearing the sum of the two is zero – the ideal bearing indeed is still. Just ahead of the bearing, however, the two waves are shifted relative to each other by a small delay time. The superposition results in a signal approximately corresponding to the differential. In **Fig. 7.30**, a correspondingly calculated superposition is juxtaposed to the measured longitudinal force. The basic shape is nicely present. It is understandable that not all small peaks are modeled: for one, band-limiting and de-convolution make for artifacts; more importantly, though, the calculation was only done for a single point: at 1 cm ahead of the bearing. In a real string, however, the mode-coupling does not only happen in a single point but across a range.

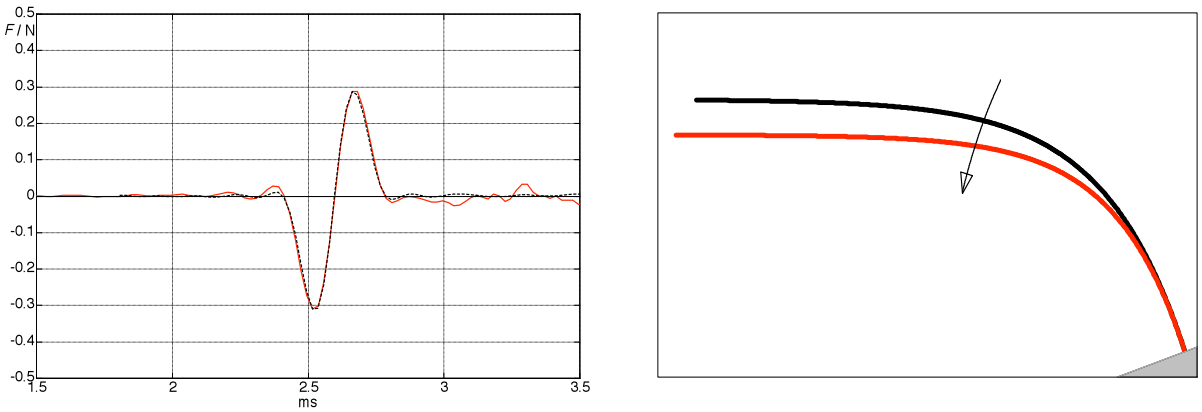

Fig. 7.30: Measured longitudinal force (——), compared to a simple model calculation (-----). On the right, the coupling between longitudinal and transversal movement is depicted.

The principle mechanism of the mode-coupling is represented by the picture on the right: pulling the string to the left at the same time results in a downward movement. Correspondingly, a downward transversal displacement makes for an additional displacement towards the left. The dependency on the sign was already shown in Fig. 7.29 – model and calculations agree well in this respect.

Fig. 7.30 shows an amplitude of the longitudinal force (force-amplitude of the dilatational wave) of 0.3 N. The particle-velocity of the dilatational wave is connected to this via the **impedance of the dilatational wave** Z_W = 16 Ns/m, yielding a velocity amplitude of the dilatational wave of 19 mm/s; that is about 7% of the velocity amplitude of the transversal wave. The **energy** of a wave depends on the square of the velocity but also on the wave impedance: $E = Z_W \cdot v^2 \cdot t$. The wave impedances for longitudinal and transverse waves differ by the factor of 30 in this case – the relation between the velocities mentioned above would therefore indicate that the energy of the longitudinal wave is about 30% of that of the transversal wave (double impulse, factor of 2!). The energy-reflection reflection, at r_E = 65%, is a little smaller in this example – the missing 5% could have been "lost" when the longitudinal wave ran across the shaker. Given the multitude of possible artifacts, this degree of precision is deemed as good.

As a summary: the more the string is curved, the higher the coupling transversal waves ⇔ longitudinal waves is. The factor of the energy coupling may be as big as 40% or more. The time functions of the waves generated by the coupling are, approximately, the derivatives of the time functions of the primary waves.

Fig. 7.31 summarizes the time-processes. A transversal velocity wave of half-sine shape is (partly) reflected as a sine-shaped longitudinal velocity wave. The latter is again (partly) reflected as a transversal velocity wave with 1.5 sine-periods. Using the derivative as an approximation becomes increasingly inaccurate as more steps in the mode-conversion are simulated. The spectral operation matching the time-derivative is a multiplication with $j\omega$, i.e. a bass-attenuation. That is why the mode-coupling has no impact for the real string in the low-frequency domain – only above 1 kHz, effects become noticeable.

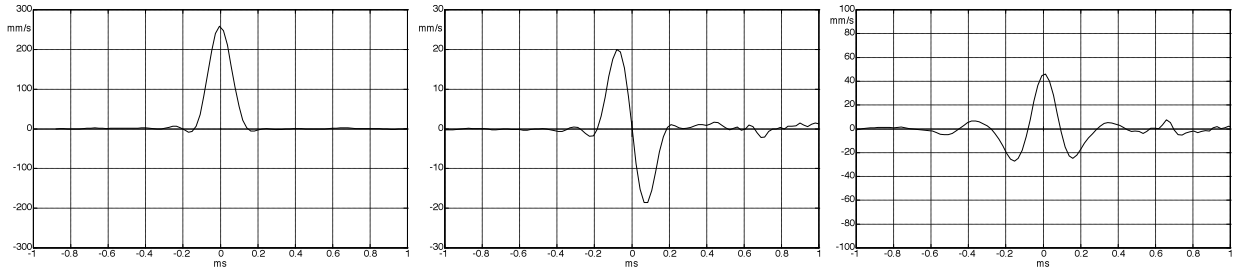

Fig. 7.31: Primary transversal wave (left), dilatational wave generated by it (middle), transversal wave generated in turn by the latter (right). All graphs are measurement results with a solid 0.7-mm-string.

For the following analyses (concentrating on **spectral effects**) the scale of the string was shortened to guitar-typical values; this was in order to get into the range of guitar-typical resonances. To enhance the effects, the string was first clamped down in a fixed manner on both ends, but then alternatively run across a knife-edge at both ends (i.e. it received a bend). The measurement with the laser-vibrometer was done at a distance of 7 mm from one of the bearings. Close to the other bearing, the string was excited with a short transversal impulse. The spectra (**Fig. 7.32**) will therefore show a **comb-filter-like shape** that depends on both the shape of the excitation impulse, and on the distance from bearing to measurement point. The high degree of correspondence between measurements and transversal-wave model indicate that for the clamped-down string, barely any dilatational waves have been generated. The spreading of the partials is the regular one, i.e. it corresponds to the theory introduced in Chapter 1.3.

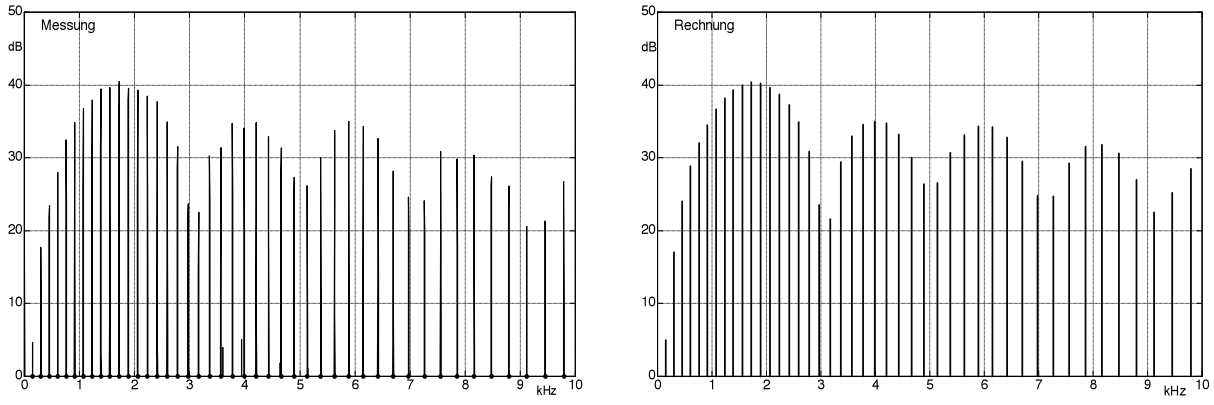

Fig. 7.32: Level-spectrum of a clamped-down 0.7-mm-string; measurement ("Messung", left) and model calculation ("Rechnung", right). The measured frequencies of the partials perfectly agree with the calculation (dots in the left-hand graph).

For the string run across the knife-edge bearings, the frequency-deviations relative to the regular spreading are evident (**Fig. 7.33**) – this is due to a stronger coupling of the mode. Both a detuning of the partials, and additional partials (e.g. around 3 kHz), can be seen.

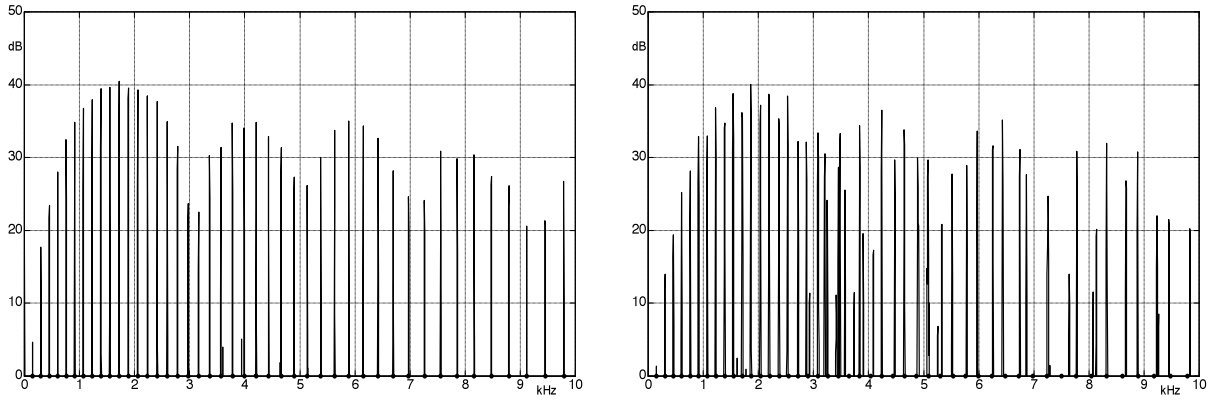

Fig. 7.33: Measured spectrum of the clamped-down string (left), and of knife-edge-supported string (right). The irregularities of the frequencies of the partials are due to the coupling of modes.

Fig. 7.34 depicts two sections from the spectrum of the knife-edge-supported string. In contrast to the clamped-down string (where the frequencies of the partials agreed with the calculated values in good approximation, Fig. 7.32), considerable deviations between calculation (dots) and measurement (line) are evident.

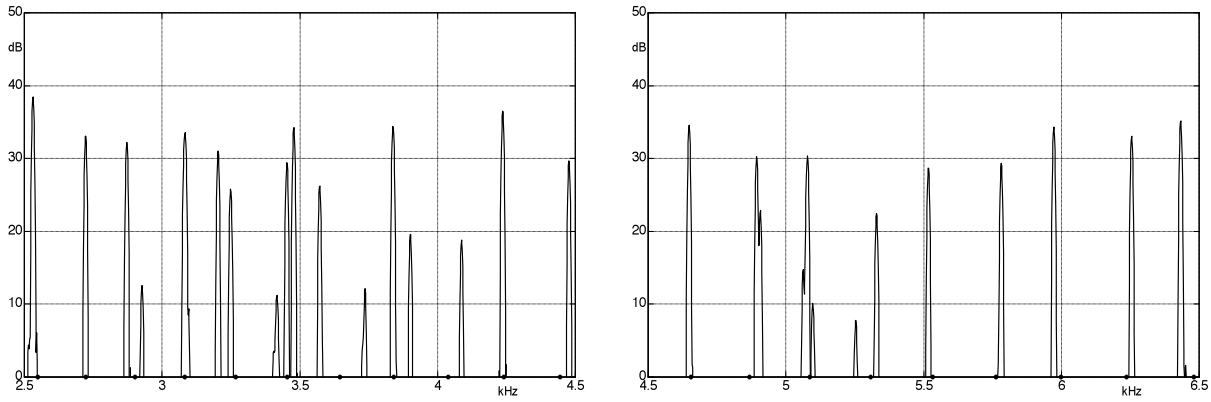

Fig. 7.34: Sections from the spectrum shown in Fig. 7.33 (right), for the knife-edge-supported string.

Of course, the question whether such effects are audible is of particular importance. Orientating **listening experiments** showed that *all* recorded velocity data sets sounded differently – however this was not due to the different string bearing but due to the non-identical excitation. Already minute differences in the plucking/picking of the string changed the spectral envelope to such an extent that differences could be heard. Therefore two sounds were synthesized that had identical spectral envelopes but different frequencies of the partials as given by Fig, 7.33. The result was that the differences in the inharmonicity are rather insignificant to the sound. Of course, it will depend on the individual case whether special beats in the partials shape the auditory impression in a particular fashion. However, from a general point-of-view, the way the string is plucked very clearly takes precedence over the inharmonicity. (See Chapter 8.2.5 for the audibility of inharmonicities in the partials).

